Electric Field Dependence of Nanoscale Cathodoluminescence succeInside Cr Doped $\beta - Ga_2O_3$ Interfaces

Dheeraj Sapkota[1], Daniel Halbing[1], John S. McCloy[2], Matthew D. McCluskey[3], Leonard J. Brillson[1,4, a)]

[1]Department of Physics, The Ohio State University, Columbus, Ohio 43210, USA

[2]School of Mechanical and Materials Engineering, Washington State University, Pullman, Washington 99164, USA

[3]Department of Physics and Astronomy, Washington State University, Pullman, Washington 99164, USA

[4]Department of Electrical and Computer Engineering, The Ohio State University, Columbus, Ohio 43210, USA

[a)] Author to whom correspondence should be addressed: brillson.1@osu.edu

ABSTRACT

Chromium (Cr) is a common impurity in $\beta - Ga_2O_3$ crystals, where its characteristic R1 and R2 luminescence lines are susceptible to both the host crystal field and externally applied fields. In this work, we demonstrate that the Cr cathodoluminescence (CL) quenches toward the bulk of the crystal but enhances with applied reverse bias, reflecting the effect of free carrier depletion with increasing electric field. Furthermore, we illustrate that the R1/R2 CL intensity ratio, measured as the integrated area ratio of R1 to R2, can be used as a direct probe of the electric field in a Ni-$\beta - Ga_2O_3$:Cr Schottky diode. This optical calibration method provides a complementary

approach to conventional C-V and I-V measurements for determining electric field strength in the depletion region of $\beta-Ga_2O_3$-based Schottky diodes and can be extended to other semiconductors and multilayer device structures.

The beta phase of gallium oxide ($\beta-Ga_2O_3$) is thermodynamically the most stable form of gallium oxide among its polymorphs[1,2,3,4] and has emerged as a promising candidate for power electronics, due to its ultra-wide bandgap (~4.8 eV) and high electric breakdown field (~8 MV/cm).[5,6] Despite these advantages, experimental studies[7,8,9,10] have consistently reported premature breakdown in $\beta-Ga_2O_3$ devices compared to theoretical predictions, which poses a significant challenge to their practical applications. Doping concentration[11,12], metal impurity diffusion, and lattice distortion resulting from interface and bulk defects[13] are usually the major factors that alter the built-in electric field distribution and contribute to early breakdown. It is, therefore, important to understand electric field distribution in $\beta-Ga_2O_3$ Schottky diodes and other heterostructure devices. Conventional characterization techniques, such as capacitance-voltage (C-V)[14,15] and current-voltage (I-V)[16] measurements, allow for the extraction of doping concentration, Schottky barrier height[17] and depletion width[18], from which the electric field is determined. However, these techniques are insufficient to measure electric fields within intermediate, nanoscale layers of heterostructure devices. Here, we demonstrate an alternative approach: using chromium cathodoluminescence as a sensitive, nanoscale gauge of built-in electric field inside $\beta-Ga_2O_3$ Schottky diodes and under applied bias.

Chromium (Cr) is an impurity in $\beta-Ga_2O_3$, introduced either intentionally or unintentionally during the melt growth method.[19,20] Cr substitutes preferentially for Ga at the octahedral Ga(II) site, forming a Cr^{3+} optical center.[21,22] The combined effect of crystal field and the spin-orbit coupling at the octahedral site split $3d^3$ orbital of Cr^{3+} into multiple sub-levels. As a result, two absorption transitions are observed ($^4A_2 \rightarrow {}^4T_2$ and $^4A_2 \rightarrow {}^4T_1$), along with a doublet emission transition ($^2E \rightarrow {}^4A_2$).[23] These characteristic emission lines, known as R1 and R2 or "red lines", appear at 696.6 nm (~1.78 eV) and 690 nm (~1.80 eV), respectively, at room temperature.[24,25]

Previous studies have shown that the luminescence of R1 and R2 lines in $\beta - Ga_2O_3$ is sensitive to external perturbations, such as pressure, temperature, and magnetic field. Barmore et al.[26] reported that in Czochralski (Cz)-grown $\beta - Ga_2O_3$, the R1-R2 splitting and their individual photoluminescence (PL) peak intensities increase significantly under both hydrostatic and non-hydrostatic pressure up to 9.2 GPa. Under non-hydrostatic conditions, the position of R1 and its integrated peak-area increase more strongly than those of R2, leading to a decreasing R2/R1 integrated peak-area ratio with pressure— evidence that R1 and R2 respond differently to applied pressure. Similarly, Remple et al.[27] studied the temperature-dependent PL of R1 and R2 in Cz-grown $\beta - Ga_2O_3$ and observed that the integrated peak-area of R1 increases more rapidly than that of R2 as temperature decreases from 300 K to 20 K. Below ~50 K, R1 dominates in both intensity and integrated peak-area due to the thermal depopulation of R2 line, again highlighting their distinct temperature dependence. In a magneto-PL spectroscopy study of Cr^{3+} in an undoped Cz-grown $\beta - Ga_2O_3$[28], Zeeman splitting of first excited state (^2E) and the ground state ($^4A_2$) was observed under a 5 T magnetic field at 5 K. Specifically, $^4A_2$ splits into four spin sublevels and ^2E of R1 into two spin sublevels, giving rise to 8 possible optical transitions for R1. Furthermore, similar splitting due to the pseudo-Stark effect has been reported in Cz-grown Cr-doped $\beta - Ga_2O_3$ under applied electric field.[23]

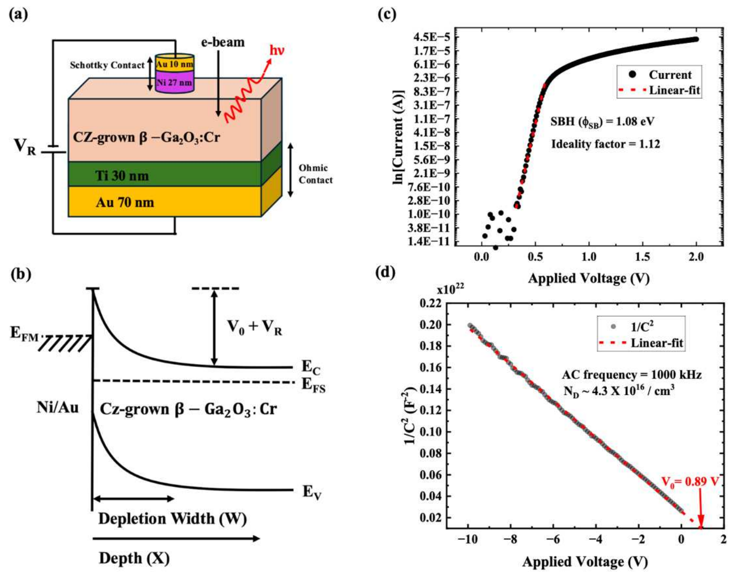

Figure 1: (a) Device schematic showing reverse biasing and the cathodoluminescence of energy $h\nu$. (b) Energy band diagram of a $Ni/Au - \beta - Ga_2O_3{:}Cr$ Schottky diode that shows band bending with applied reverse bias (V_0 +V_R) and the depletion width (W). E_{FM} and E_{FS} represent the Fermi level in Ni/Au and $\beta - Ga_2O_3{:}Cr$ regions, respectively. (c) ln(I) – forward bias (V) characteristics of the diode that provides the Schottky barrier height (SBH) and the ideality factor. (d) $1/C^2$ – reverse bias (V_R) characteristics of the diode that provides the built-in band bending (V_0) and the effective donor concentration (N_D).

$\beta - Ga_2O_3{:}Cr$ crystals were grown by the Czochralski method[29,30,31] at Washington State University, Institute of Materials Research.[32] Cr concentration was batched at 0.05 atomic % from a 3N7 (99.97%) purity Cr_2O_3 precursor and 5N (99.999%) purity $\beta - Ga_2O_3$. The Ni/Au Schottky contacts were patterned on the (100) $\beta - Ga_2O_3$ using a Heidelberg MLA150, and the metals were deposited via e-beam evaporation with a CHA Solution System E-Gun Evaporator at NanoTech

West, Ohio State University (OSU). An array of circular Schottky contacts with diameters ranging 75 - 350 micrometers was deposited. Ni was 27 nm thick, capped with a 10 nm Au layer to prevent oxidation and to provide a good electrical contact during biasing. Figure 1(a) shows a representative Schottky contact with a diameter of 350 μm. The Ti/Au Ohmic contact was unpatterned, instead deposited to cover entire substrate backside using e-beam evaporation at AFRL, Dayton, Ohio. The diode was biased with a 2400 Keithley Sourcemeter. The biasing was performed in an ultra-high vacuum (UHV) environment. Capacitance-Voltage (C-V) measurements were taken with an HP 4192A LF Impedance Analyzer at an input ac frequency of a 1000 kHz. Depth-resolved Cathodoluminescence Spectroscopy (DRCLS) was performed in an UHV 7800F JEOL JAMP Scanning Electron Microscope. Figure 1(b) shows the schematic of a Ni/Au-$\beta - Ga_2O_3{:}Cr$ energy band bending and the depletion width under the applied reverse bias condition.

All diodes investigated in this work were initially forward biased from 0 V to 2 V to confirm Schottky barrier turn-on. Figure 1(c) shows the current-voltage (I-V) characteristics of a representative diode in a semi-logarithmic plot. From the slope and the intercept of the linear fit, the Schottky barrier height (SBH) and the ideality factor were computed as 1.08 eV and 1.12, respectively. The obtained SBH is in close agreement with the theoretical Schottky-Mott limit[33] and previous experimental works.[34,35,36] Subsequently, the capacitance-voltage (C-V) characteristics were measured under reverse bias. Analysis of $1/C^2$ versus reverse bias (-V) plot yielded a built-in potential of 0.89 V and an effective donor concentration of approximately $4.3 \times 10^{16}\ /cm^3$, as shown in Fig. 1(d).

Fig. 2(a) shows the depth-resolved cathodoluminescence spectroscopy (DRCLS)[37,38,39] of a Cz-grown $\beta - Ga_2O_3{:}Cr$ under no-bias conditions. The Bohr-Bethe penetration depth (R_B)[40] was estimated from a Monte Carlo depth simulation program, CASINO, and the spectra were deconvolved using the MagicPlot program. The deconvolution shown for the R_B=2 nm spectrum reveals Cr emission lines, R1 and R2, centered at 1.74 eV and 1.78 eV, respectively. Their peaks in Ga_2O_3 are typically expected at 1.78 eV and 1.80 eV, respectively.[27] The observed deviation in the R1 and R2 peak energies likely arises from deconvolution uncertainties, charged-coupled device (CCD) calibration, or ambient conditions during the measurements.

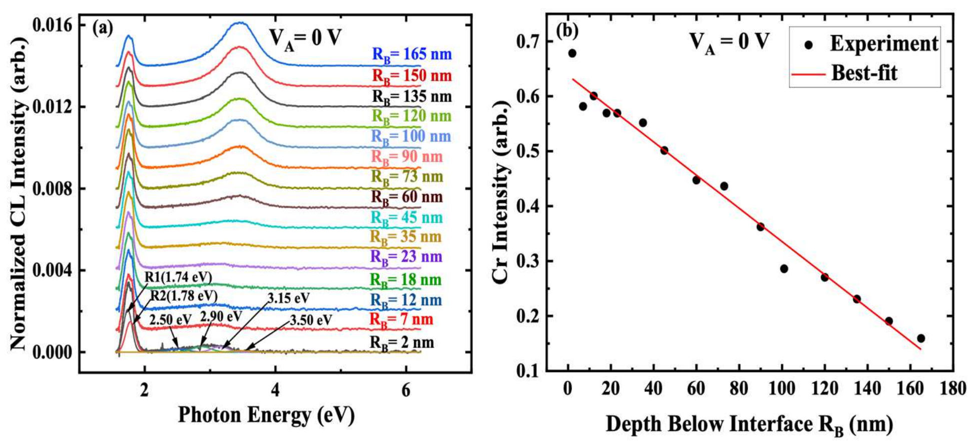

Figure 2: (a) Depth-resolved Cathodoluminescence Spectroscopy (DRCLS) of $\beta - Ga_2O_3{:}\,Cr$ under zero reverse bias condition. R_B represents the Bohr-Bethe penetration depth below the interface. Deconvolution of the spectra is shown for R_B= 2 nm. (b) The Cr intensity, defined as the sum of integrated peak areas of R1 and R2 emissions, normalized by the total integrated area of the corresponding spectrum, and plotted as a function of depth below the interface.

In addition to Cr-related emissions, higher energy emissions are observed at 2.5 eV, 2.90 eV, 3.15 eV, and 3.50 eV. Based on previous experimental reports[41,42,43] and theoretical expectations[44,45], 2.5 eV is attributed to a gallium vacancy complexed with hydrogen (V_{Ga}-H), 2.90 eV and 3.15 eV to gallium vacancy (V_{Ga}) complexes, and 3.50 eV to oxygen vacancies (V_O).

Since this work centers on Cr-related cathodoluminescence, we restrict our discussion to only the R1 and R2 peaks. As shown in Fig. 2(b), the Cr intensity, defined as the sum of integrated peak areas of R1 and R2 and normalized by the total integrated area of the corresponding spectrum, decreases with increasing penetration depth. This suggests either (i) Cr segregation toward the interface, (ii) free carrier depletion effects,[46] or (iii) a proportional decrease of the 2.5 – 3.6 eV defect intensities. Furthermore, the Cr intensity at a specific depth below the interface increases under reverse bias, which is shown in the supplementary materials, Fig. S2. The applied reverse bias widens the depletion region and pushes free carriers (electrons) away from the interface. Consequently, the local free carrier concentration decreases at this depth, leading to enhanced Cr emission. This observation supports the free carrier depletion effect proposed in (ii).

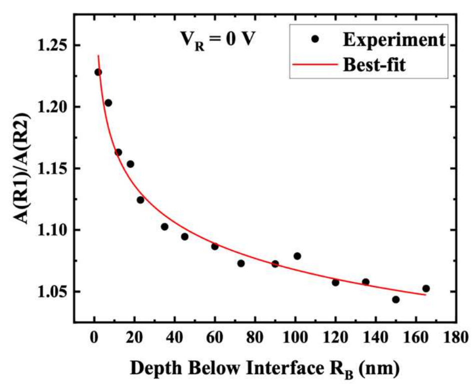

Figure 3: Ratio of integrated peak-area of R1 to R2, A(R1)/A(R2), as function of depth under zero applied bias (V_R= 0 V). The ratio decreases with increasing depth and follows a power-law decay equation of the form ax^{-b}.

We investigate the relative intensity of the R1 and R2 through the integrated peak area ratio, A(R1)/A(R2), versus depth below the interface. As shown in Fig. 3, the ratio is largest near the interface and decreases with increasing depth under zero applied bias. The ratio approaches almost unity at the end of the depletion region (W= 167 nm), which indicates that the relative contributions of R1 and R2 become nearly equal. This trend suggests that the R1 emission is more prominent in the regions of stronger built-in electric field near the interface and decreases more rapidly with depth compared to R2, likely reflecting a stronger influence of free carriers and the electric field in the bulk on R1. The depth dependence of the ratio is best described by a power-law decay of the form $A(R1)/A(R2) = ax^{-b}$, with $a = 1.276 \pm 0.009$ and $b = 0.039 \pm 0.002$, where x is the depth below the interface.

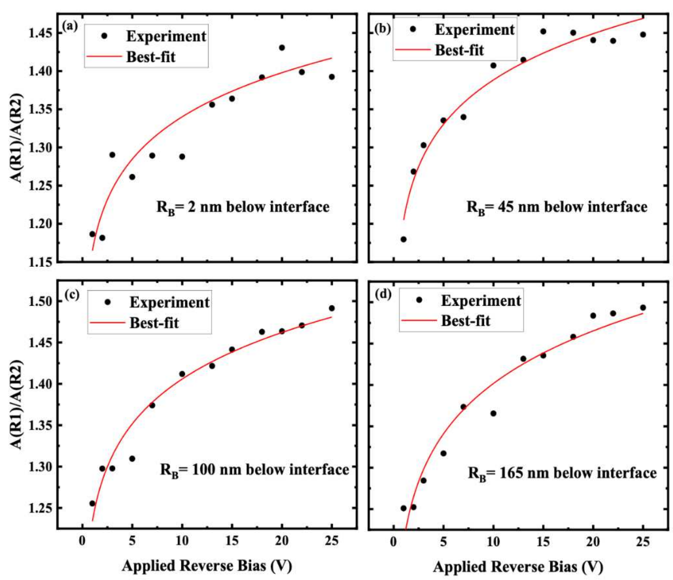

Figure 4: Ratio of integrated peak area of R1 to R2, A(R1)/A(R2), as a function of applied reverse bias at (a) 2 nm (b) 45 nm (c) 100 nm and (d) 165 nm below the interface.

To further examine the field effect, we study the reverse bias dependence of R1/R2 intensity ratio at different depths below the interface. As shown in Fig. 4, the ratio increases with increasing reverse bias, which can be attributed to the effect of increased free carrier depletion with higher reverse bias at a given depth. As R1/R2 ratio increases with the reverse bias, the rate of increase is higher for R1 than R2, which suggests that R1 emission is more sensitive to and increases faster with the electric field than R2.

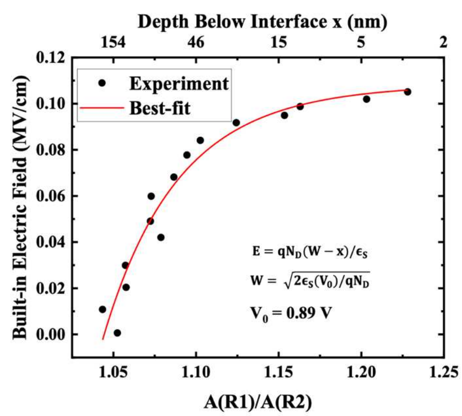

Figure 5: A calibration of the built-in electric field in the depletion region as a function of R1 and R2 peak area ratio. The electric field is approximated to follow a power law equation with A(R1)/A(R2) of the form A-Bx^{-C}. The data in Fig. 5 originates from Fig. 3.

The systematic variation of R1/R2 intensity ratio with the depth and applied reverse bias confirms that the ratio provides a direct optical signature of electric field in $\beta-Ga_2O_3$: Cr. In the following discussion, we show that the built-in and applied electric fields can be estimated from the measured R1/R2 intensity ratio. In particular, the electric field in a semiconductor is $qN_D(W-x)/\epsilon_S$, where q is the free carrier charge, N_D is the effective donor concentration, W is the depletion width, x is the depth, and ϵ_S is the dielectric permittivity. By combining the depth dependence A(R1)/A(R2) with the electric field distribution, the electric field is written as $E = \left(E_{max} - \xi\left(\frac{A(R1)}{A(R2)}\right)^{-1/b}\right)$, where $E_{max} = qN_D W/\epsilon_S$ and $\xi = qN_D a^{\frac{1}{b}}/\epsilon_S$.

Fig. 5 shows the variation of the electric field as a function of A(R1)/A(R2). The data are well described by a best-fit equation of the form $A - Bx^{-C}$, with $A = 0.108 \pm 0.007$ MV/cm, $B = 0.295 \pm 0.006$ MV/cm and $C = 23.01 \pm 4.40$, which are in excellent agreement with the expected E_{max} , ξ and 1/b, respectively. The results indicate that higher electric field corresponds to a larger R1/R2 ratio, implying that R1 emission increases more than R2 with increasing electric field. This non-linear response of the measured R1/R2 intensity ratio can therefore be utilized as a tool to measure the built-in electric field in $\beta - Ga_2O_3$, reducing the need for depletion width measurements and the effective donor concentration in determining a Schottky diode's electric field. Furthermore, in Fig. S3 of supplementary materials, we present the calibration of the applied electric field with the measured R1/R2 intensity ratio at different depths. The ratio shows a linear response to the applied electric field, which further confirms that R1 emission increases faster with electric field than R2. The established calibration thus enables the measurement of applied electric field with optical emission of Cr R1/R2 relative intensity without the need for the electrical contact-based measurements.

In summary, we investigated the depth and reverse bias dependence of Cr cathodoluminescence in a Cz-grown $\beta - Ga_2O_3$: Cr Schottky diode. The quenching of Cr intensity and the corresponding change in the R1/R2 intensity ratio in the bulk, along with their enhancement under applied reverse bias at a particular depth indicate that the free carrier depletion plays a key role in governing the Cr emission.

In general, experimental parameters affect the intensities of the R1 and R2 lines differently and cannot be explained merely by the equilibrium occupations of the two levels. The splitting between R1 and R2 is governed by spin-orbit and crystal field effects. Hydrostatic pressure perturbs the interaction between Cr^{3+} and the crystal field, causing changes in nonradiative recombination rates for the R1 and R2 states.[26] Temperature has a similar effect due to electron-phonon coupling.[27] Alloying and nonhydrostatic stress also affect the levels, with the R1 response stronger than that of R2.[27,26] The present work adds electric field to the class of external perturbations for which R1 is more sensitive than R2.

We have shown that the intensity ratio can be utilized as a tool to measure the electric field in $\beta-Ga_2O_3$ devices, establishing a direct optical calibration of electric field strength without requiring separate measurements of depletion width and donor concentration. Whereas conventional C-V and I-V techniques lack 3-dimensional spatial resolution, Fig. 5 shows that β-Ga_2O_3[47] as well other materials such as Al_2O_3[48,49], GaAs[50,51,52,53,54], and GaN[55] can be probed by the R1/R2 CL intensity ratio technique since Cr can be intentionally doped or it occurs naturally as an impurity. This approach offers applications for characterizing electric field gradients associated with dielectric breakdown in $\beta-Ga_2O_3$ diodes as well as other Ga-based semiconductor interfaces since Cr is a common impurity in Ga source material for growth,[13,19,25] and the DRCLS technique enables electric field gradient characterization across and inside metal/ $\beta-Ga_2O_3$ diodes spatially on a nanoscale in three dimensions. Beyond $\beta-Ga_2O_3$ Schottky diodes, insertion of Cr fractional monolayers near other semiconductor heterojunction quantum wells could provide direct measurement of electric field gradients that can spatially separate electrons and holes inside quantum wells, which would degrade their absorption, recombination and light output.[56] More generally, spatial distribution measurements of electric field gradients within and across semiconductor devices could influence nanoscale device design.

SUPPLEMENTARY MATERIAL

Additional experimental details, including Monte Carlo simulations, cathodoluminescence spectra and Cr intensity under reverse bias conditions, applied electric field calibration with R1/R2 intensity ratio, and best-fit parameters of electric field vs. R1/R2 intensity ratio.

ACKNOWLEDGEMENTS

L.J.B. and D.S. acknowledge diode fabrications facilities from Ohio State University's Nanotechnology West Laboratory and support by the Department of Energy, Office of Basic Energy Sciences, Division of Materials Science and Engineering under Award. DE-SC0025601, Materials Sciences and Engineering Division. M.D.M. acknowledges experimental assistance from Cassandra Remple and support by the Department of Energy, Office of Basic Energy Sciences, Division of Materials Science and Engineering under Award No. DE-FG02-07ER46386.

AUTHOR DECLARATIONS

Conflict of Interest

The authors have no conflicts to disclose.

Author Contributions

D. Sapkota: Device design (lead); Metal contacts deposition (lead); Data acquisition (lead); Data analysis (lead); Writing— original draft (lead); Writing— review and editing (lead). **D. Halbing**: Data acquisition (supporting); Data analysis (supporting); Writing— review and editing (supporting). **J.S. McCloy**: Substrate growth (lead); Writing— review and editing (supporting).

M.D. McCluskey: Substrate growth (equal); Writing— review and editing (supporting); Conceptualization (supporting). **L.J. Brillson**: Conceptualization (lead); Methodology (lead); Funding acquisition (lead); Data analysis (supporting); Writing— original draft (supporting); Writing— review and editing (supporting).

DATA AVAILABILITY

The data that support the findings of this study are available within the supplementary information and from the corresponding author upon reasonable request.

REFERENCES

[1] Higashiwaki, M., and Fujita, S. (Eds.), "*Gallium Oxide: Materials Properties, Crystal Growth, and Devices", Springer Nature*, **293**, 2-5 (2020).
DOI: https://doi.org/10.1007/978-3-030-37153-1

[2] Roy, R., Hill, V. G., and Osborn, E. F., "Polymorphism of Ga_2O_3 and the system Ga_2O_3—H_2O", *Journal of the American Chemical Society*, **74**(3), 719-722 (1952).
DOI: https://doi.org/10.1021/ja01123a039

[3] Pearton, S. J., Yang, J., Cary, P. H., Ren, F., Kim, J., Tadjer, M. J., and Mastro, M. A., "A review of Ga_2O_3 materials, processing, and devices", *Applied Physics Reviews*, **5**(1), 011301 (2018).
DOI: https://doi.org/10.1063/1.5006941

[4] Green, A.J., Speck, J., Xing, G., Moens, P., Allerstam, F., Gumaelius, K., Neyer, T., Arias-Purdue, A., Mehrotra, V., Kuramata, A., Sasaki, K., Watanabe, S., Koshi, K., Blevins, J., Bierwagen, O., Krishnamoorthy, S., Leedy, K., Arehart, A.R., Neal, A.T., Mou, S., Ringel, S.A., Kumar, A.,

Sharma, A., Ghosh, K., Singisetti, U., Li, W., Chabak, K., Liddy, K., Islam, A., Rajan, S., Graham, S., Choi, S., Cheng, Z. and Higashiwaki, M., "β-Gallium oxide power electronics", *Apl Materials*, *10*(2), 029201 (2022).

DOI: https://doi.org/10.1063/5.0060327

[5] Higashiwaki, M., Sasaki, K., Kuramata, K., Masui, T., and Yamakoshi, S., "Development of gallium oxide power devices", *physica status solidi (a)*, **211**(1), 21-26 (2014).

DOI: https://doi.org/10.1002/pssa.201330197

[6] Higashiwaki, M., Sasaki, K., Murakami, H., Kumagai, Y., Koukitu, A., Kuramata, A., Masui, T., and Yamakoshi, S., "Recent progress in Ga_2O_3 power devices", *Semiconductor Science and Technology*, *31*(3), 034001 (2016).

DOI: 10.1088/0268-1242/31/3/034001

[7] Yang, J., Ahn, S., Ren, F., Pearton, S. J., Jang, S., and Kuramata, A., "High breakdown voltage (−201) $\beta - Ga_2O_3$ Schottky rectifiers", *IEEE Electron Device Letters*, *38*(7), 906-909 (2017).

DOI: 10.1109/LED.2017.2703609

[8] Konishi, K., Goto, K., Murakami, H., Kumagai, Y., Kuramata, A., Yamakoshi, S., and Higashiwaki, M., "1-kV vertical Ga_2O_3 field-plated Schottky barrier diodes", *Applied Physics Letters*, *110*(10), 103506 (2017).

DOI: https://doi.org/10.1063/1.4977857

[9] Yang, J., Ahn, S., Ren, F., Pearton, S. J., Jang, S., Kim, J., and Kuramata, A., "High reverse breakdown voltage Schottky rectifiers without edge termination on Ga_2O_3", *Applied Physics Letters*, *110*(19), 192101 (2017).

DOI: https://doi.org/10.1063/1.4983203

[10] Dhara, S., Kalarickal, N. K., Dheenan, A., Joishi, C., and Rajan, S., "β-Ga_2O_3 Schottky barrier diodes with 4.1 MV/cm field strength by deep plasma etching field-termination", *Applied Physics Letters*, *121*(20), 203501 (2022).

DOI: https://doi.org/10.1063/5.0123284

[11] Baliga, B. J., "Fundamentals of power semiconductor devices", Springer, 107-118 (2018).

ISBN: 3319939874

[12] Sasaki, K., Higashiwaki, M., Kuramata, A., Masui, T., and Yamakoshi, S., "$\beta - Ga_2O_3$ Schottky Barrier Diodes Fabricated by Using Single-Crystal $\beta - Ga_2O_3$ (010) Substrates", *IEEE electron device letters*, *34*(4), 493-495 (2013).

DOI: 10.1109/LED.2013.2244057

[13] Ramdin, D. N., Huang, H. L., Chae, C., Dhara, S., Rajan, S., Hwang, J., and Brillson, L. J., "Impact of metal diffusion, lattice distortions, native defects, and ambient on dielectric breakdown in Ni–Ga_2O_3 Schottky diodes", *APL Materials*, *12*(10), 101118 (2024).

DOI: https://doi.org/10.1063/5.0228825

[14] Zhang, S., Liu, Z., Liu, Y., Zhi, Y., Li, P., Wu, Z., and Tang, W., "Electrical characterizations of planar Ga_2O_3 Schottky barrier diodes", *Micromachines*, *12*(3), 259 (2021).

DOI: https:// doi.org/10.3390/mi12030259

[15] Bryant, F. J., Majid, J. M., Scott, C. G., and Shaw, D., "The interpretation of non-linear Schottky barrier C^{-2} -V characteristics", *Solid state communications*, *63*(1), 9-12 (1987).

DOI: https://doi.org/10.1016/0038-1098(87)90055-X

[16] Sze, S. M., "*Semiconductor devices: physics and technology*", *John wiley & sons*, Second edition, pp. 232 (2008).

ISBN: 812651681X

[17] Tung, R. T., "The physics and chemistry of the Schottky barrier height", *Applied Physics Reviews*, **1**(1), 011304 (2014).

DOI: http://dx.doi.org/10.1063/1.4858400

[18] Takshi, A., Dimopoulos, A., and Madden, J. D., "Depletion width measurement in an organic Schottky contact using a metal-semiconductor field-effect transistor", *Applied Physics Letters*, *91*(8), 083513 (2007).

DOI: https://doi.org/10.1063/1.2773953

[19] Kuramata, A., Koshi, K., Watanabe, S., Yamaoka, Y., Masui, T., and Yamakoshi, S., "High-quality β-Ga_2O_3 single crystals grown by edge-defined film-fed growth", *Japanese Journal of Applied Physics*, *55*(12), 1202A2 (2016).

DOI: https://doi.org/10.7567/JJAP.55.1202A2

[20] Galazka, Z., Ganschow, S., Fiedler, A., Bertram, R., Klimm, D., Irmscher, K., Schewski, R., Pietsch, M., Albrecht, M. and Bickermann, M., "Doping of Czochralski-grown bulk β-Ga_2O_3 single crystals with Cr, Ce and Al", *Journal of Crystal Growth*, *486*, 82-90 (2018).

DOI: https://doi.org/10.1016/j.jcrysgro.2018.01.022

[21] Vivien, D., Viana, B., Revcolevschi, A., Barrie, J. D., Dunn, B., Nelson, P., and Stafsudd, O. M., "Optical properties of β-Ga_2O_3: Cr^{3+} single crystals for tunable laser applications", *Journal of luminescence*, *39*(1), 29-33 (1987).

DOI: https://doi.org/10.1016/0022-2313(87)90006-8

[22] Turiansky, M.E., Mu, S., Razinkovas, L., Parto, K., Patel, S.D., Doan, S., Pokharel, G., Gomez Alvarado, S.J., Wilson, S.D., Moody, G. and Van de Walle, C.G., "Characterization of chromium impurities in β-Ga_2O_3", *Journal of Applied Physics*, *137*(10),104401 (2025).

DOI: https://doi.org/10.1063/5.0255859

[23] Fiedler, A., Galazka, Z., and Irmscher, K., "Electroluminescence of Cr^{3+} and pseudo-Stark effect in β-Ga_2O_3 Schottky barrier diodes", *Journal of Applied Physics*, *126*(21), 213104 (2019).
DOI: https://doi.org/10.1063/1.5125774

[24] Tippins, H. H., "Optical and microwave properties of trivalent chromium in β-Ga_2O_3", *Physical Review*, *137*(3A), A865 (1965).
DOI: https://doi.org/10.1103/PhysRev.137.A865

[25] Luchechko, A., Vasyltsiv, V., Zhydachevskyy, Y., Kushlyk, M., Ubizskii, S., and Suchocki, A., "Luminescence spectroscopy of Cr^{3+} ions in bulk single crystalline β-Ga_2O_3", *Journal of Physics D: Applied Physics*, *53*(35), 354001 (2020).
DOI: https://doi.org/10.1088/1361-6463/ab8c7d

[26] Barmore, L. M., Jesenovec, J., McCloy, J. S., and McCluskey, M. D., "Photoluminescence of Cr^{3+} in β-Ga_2O_3 and $(Al_{0.1}Ga_{0.9})_2O_3$ under pressure", *Journal of Applied Physics*, *133*(17), 175703 (2023).
DOI: https://doi.org/10.1063/5.0149900

[27] Remple, C., Barmore, L. M., Jesenovec, J., McCloy, J. S., and McCluskey, M. D., "Photoluminescence spectroscopy of Cr^{3+} in β-Ga_2O_3 and $(Al_{0.1}Ga_{0.9})_2O_3$", *Journal of Vacuum Science & Technology A*, *41*(2), 022702 (2023).
DOI: https://doi.org/10.1116/6.0002340

[28] Stehr, J. E., Jansson, M., Hofmann, D. M., Kim, J., Pearton, S. J., Chen, W. M., and Buyanova, I. A., "Magneto-optical properties of Cr^{3+} in β-Ga_2O_3", *Applied Physics Letters*, *119*(5), 052101 (2021).
DOI: https://doi.org/10.1063/5.0060628

[29] Galazka, Z., Irmscher, K., Uecker, R., Bertram, R., Pietsch, M., Kwasniewski, A., Naumann, M., Schulz, T., Schewski, R., Klimm, D. and Bickermann, M., "On the bulk β-Ga_2O_3 single crystals grown by the Czochralski method", *Journal of Crystal Growth*, *404*, 184-191 (2014).

DOI: https://doi.org/10.1016/j.jcrysgro.2014.07.021

[30] Galazka, Z., "Growth of bulk β-Ga_2O_3 single crystals by the Czochralski method", *Journal of Applied Physics*, *131*(3), 031103 (2022).

DOI: https://doi.org/10.1063/5.0076962

[31] Irmscher, K., Galazka, Z., Pietsch, M., Uecker, R., and Fornari, R., "Electrical properties of β-Ga_2O_3 single crystals grown by the Czochralski method", *Journal of Applied Physics*, *110*(6), 063720 (2011).

DOI: https://doi.org/10.1063/1.3642962

[32] McCloy, J.S., Jesenovec, J., Dutton, B.L., Pansegrau, C., Remple, C., Weber, M.H., Swain, S., McCluskey, M. and Scarpulla, M., "Growth and defect characterization of doped and undoped β-Ga_2O_3 crystals", *Oxide-based Materials and Devices XIII,* edited by Teherani, F.H. and Rogers, D.J., *SPIE,* 12002, 21-39 (2022).

DOI: https://doi.org/ 10.1117/12.2611852

[33] Tung, R. T., "Recent advances in Schottky barrier concepts", *Materials Science and Engineering: R: Reports*, *35*(1-3), 1-138 (2001).

DOI: https://doi.org/10.1016/S0927-796X(01)00037-7

[34] Yao, Y., Gangireddy, R., Kim, J., Das, K. K., Davis, R. F., and Porter, L. M. (2017), "Electrical behavior of β-Ga_2O_3 Schottky diodes with different Schottky metals", *Journal of Vacuum Science & Technology B*, *35*(3), 03D113 (2017).

DOI: https://doi.org/10.1116/1.4980042

---

[35] Jiang, K., Lyle, L.A., Favela, E., Moody, D., Lin, T., Das, K.K., Popp, A., Galazka, Z., Wagner, G. and Porter, L.M., "Electrical properties of (100) β-Ga_2O_3 Schottky diodes with four different metals", *ECS Transactions*, *92*(7), 71 (2019).

DOI: https://doi.org/10.1149/09207.0071ecst

[36] Zhang, S., Liu, Z., Liu, Y., Zhi, Y., Li, P., Wu, Z., and Tang, W., "Electrical characterizations of planar Ga_2O_3 Schottky barrier diodes", *Micromachines*, *12*(3), 259 (2021).

DOI: https://doi.org/10.3390/mi12030259

[37] Brillson, L. J., "Applications of depth-resolved cathodoluminescence spectroscopy", *Journal of Physics D: Applied Physics*, *45*(18), 183001 (2012).

DOI: https://doi.org/10.1088/0022-3727/45/18/183001

[38] Brillson, L. J., "*An essential guide to electronic material surfaces and interfaces*", John Wiley & Sons, New York, Chapter 11.10, 181-189 (2016).

ISBN: 978-1119027119

[39] Brillson, L.J., "Surfaces and interfaces of electronic materials", Wiley and IEEE, 279-293 (2010).

ISBN: 978-3527409150

[40] Everhart, T. E., and Hoff, P. H., "Determination of kilovolt electron energy dissipation vs penetration distance in solid materials", *Journal of Applied Physics*, *42*(13), 5837-5846 (1971).

DOI: https://doi.org/10.1063/1.1660019

[41] Gao, H., Muralidharan, S., Pronin, N., Karim, M.R., White, S.M., Asel, T., Foster, G., Krishnamoorthy, S., Rajan, S., Cao, L.R., Higashiwaki, M., Wenckstern, H.V., Grundmann, M., Zhao, H., Look, D.C., and Brillson L.J., "Optical signatures of deep level defects in Ga_2O_3", *Applied Physics Letters*, *112*(24), 242101 (2018).

DOI: https://doi.org/10.1063/1.5026770

[42] Ramdin, D. N., Haseman, M. S., Huang, H. L., Leedy, K. D., Hwang, J., and Brillson, L. J., "Optical and electronic effects of rapid thermal annealing at Ir–Ga_2O_3 interfaces", *Journal of Applied Physics*, *131*(20), 205302 (2022).

DOI: https://doi.org/10.1063/5.0090161

[43] McCluskey, M. D., "Point defects in Ga_2O_3", *Journal of Applied Physics*, *127*(10), 101101 (2020).

DOI: https://doi.org/10.1063/1.5142195

[44] Peelaers, H., Lyons, J. L., Varley, J. B., and Van de Walle, C. G., "Deep acceptors and their diffusion in Ga_2O_3", *APL Materials*, *7*(2), 022519 (2019).

DOI: https://doi.org/10.1063/1.5063807

[45] Frodason, Y. K., Johansen, K. M., Vines, L., and Varley, J. B., "Self-trapped hole and impurity-related broad luminescence in β-Ga_2O_3", *Journal of Applied Physics*, *127*(7), 075701 (2020).

DOI: https://doi.org/10.1063/1.5140742

[46] Remple, C., Dutton, B. L., Varley, J. B., McCloy, J. S., and McCluskey, M. D., "Cr is not an acceptor in β-Ga_2O_3", *Physical Review Materials*, *9*(5), 054606 (2025).

DOI: https://doi.org/10.1103/PhysRevMaterials.9.054606

[47] Higashiwaki, M., and Wong, M. H., "Beta-gallium oxide material and device technologies", *Annual Review of Materials Research*, *54*(1), 175-198 (2024).

DOI: https://doi.org/10.1146/annurev-matsci-080921-104058

[48] Seat, H. C., and Sharp, J. H., "Dedicated temperature sensing with c-axis oriented single-crystal ruby (Cr^{3+}: Al_2O_3) fibers: temperature and strain dependences of R-line fluorescence", *IEEE Transactions on Instrumentation and Measurement*, *53*(1), 140-154 (2004).

DOI: 10.1109/TIM.2003.822010

[49] Schawlow, A. L., "Fine-Line Spectra of Chromium Ions in Crystals", *Journal of Applied Physics*, *33*(1), 395-398 (1962).

DOI: https://doi.org/10.1063/1.1777130

[50] Ledebo, L. A., and Ridley, B. K., "On the position of energy levels related to transition-metal impurities in III-V semiconductors", *Journal of Physics C: Solid State Physics*, *15*(27), L961 (1982).

DOI: 10.1088/0022-3719/15/27/003

[51] Look, D. C., "On the interpretation of photoconductivity and photo-hall spectra in semi-insulating GaAs: Cr", *Solid State Communications*, *24*(12), 825-828 (1977).

DOI: https://doi.org/10.1016/0038-1098(77)91222-4

[52] Deveaud, B., Picoli, G., Lambert, B., and Martinez, G., "Luminescence processes at chromium in GaAs", *Physical Review B*, *29*(10), 5749 (1984).

DOI: https://doi.org/10.1103/PhysRevB.29.5749

[53] Mönch, W., Clemens, H. J., Görlich, S., Enninghorst, R., and Gant, H., "Surface photovoltage spectroscopy with cleaved GaAs (110) surfaces: Spectroscopy of Cr^{2+}", *Journal of Vacuum Science and Technology*, *19*(3), 525-530 (1981).

DOI: https://doi.org/10.1116/1.571119

[54] Eaves, L., Williams, P. J., and Uihlein, C., "The observation of a sharp peak in the deep-level photoconductivity spectrum of GaAs (Cr) due to the Cr^{2+} ($^5T_2$-^5E) 'intracentre' transition", *Journal of Physics C: Solid State Physics*, *14*(23), L693 (1981).

DOI: 10.1088/0022-3719/14/23/004

[55] Toth, M., and Phillips, M. R., "Detection of Cr impurities in GaN by room temperature cathodoluminescence spectroscopy", *Applied Physics Letters*, *75*(25), 3983-3985 (1999).
DOI: https://doi.org/10.1063/1.125528

[56] Miller, D., Weiner, J., and Chemla, D., "Electric-field dependence of linear optical properties in quantum well structures: Waveguide electroabsorption and sum rules", *IEEE Journal of Quantum Electronics*, *22*(9), 1816-1830 (1986).
DOI: 10.1109/JQE.1986.1073167